NeuroImage 46 (2009) 382–393

Contents lists available at ScienceDirect

NeuroImage

journal homepage: www.elsevier.com/locate/ynimg

Target-specific contrast agents for magnetic resonance microscopy

Megan L. Blackwell [a,b,*], Christian T. Farrar [a,d], Bruce Fischl [a,c,d], Bruce R. Rosen [a,d]

[a] Athinoula A. Martinos Center for Biomedical Imaging, Charlestown, MA, USA
[b] Harvard-MIT Division of Health Sciences and Technology, Cambridge, MA, USA
[c] Computer Science and Artificial Intelligence Laboratory, MIT, Cambridge, MA, USA
[d] Department of Radiology, Massachusetts General Hospital, Charlestown, MA, USA

ARTICLE INFO

Article history:
Received 2 July 2007
Revised 5 December 2008
Accepted 15 January 2009
Available online 30 January 2009

ABSTRACT

High-resolution *ex vivo* magnetic resonance (MR) imaging can be used to delineate prominent architectonic features in the human brain, but increased contrast is required to visualize more subtle distinctions. To aid MR sensitivity to cell density and myelination, we have begun the development of target-specific paramagnetic contrast agents. This work details the first application of luxol fast blue (LFB), an optical stain for myelin, as a white matter-selective MR contrast agent for human *ex vivo* brain tissue. Formalin-fixed human visual cortex was imaged with an isotropic resolution between 80 and 150 μm at 4.7 and 14 T before and after *en bloc* staining with LFB. Longitudinal (R1) and transverse (R2) relaxation rates in LFB-stained tissue increased proportionally with myelination at both field strengths. Changes in R1 resulted in larger contrast-to-noise ratios (CNR), per unit time, on T1-weighted images between more myelinated cortical layers (IV–VI) and adjacent, superficial layers (I–III) at both field strengths. Specifically, CNR for LFB-treated samples increased by 229 ± 13% at 4.7 T and 269 ± 25% at 14 T when compared to controls. Also, additional cortical layers (IVca, IVd, and Va) were resolvable in 14T-MR images of LFB-treated samples but not in control samples. After imaging, samples were sliced in 40-micron sections, mounted, and photographed. Both the macroscopic and microscopic distributions of LFB were found to mimic those of traditional histological preparations. Our results suggest target-specific contrast agents will enable more detailed MR images with applications in imaging pathological *ex vivo* samples and constructing better MR atlases from *ex vivo* brains.

Introduction

High-field magnetic resonance (MR) microscopy is emerging as a powerful tool for studying the microstructure of many tissues, including the cytoarchitecture of the human brain (Augustinack et al., 2005; Hinds et al., 2008). However, conventional MR is restricted by the relatively small inherent differences in relaxation rates, and hence image contrast, of different tissues. While *in vivo* T1-weighted images are sensitive to laminar differences in archicortex (Press et al., 1989; Damasio et al., 1991) and in neocortex (Walters et al., 2003; Barbier et al., 2002; Clare and Bridge, 2005), T1-weighted images of formalin-fixed brains display very low contrast, even between gray and white matter (Oros-Peusquens et al., 2003). Some groups (Johnson et al., 2002) have used gadolinium-based contrast agents to enhance high-resolution images of *ex vivo* rodents, but these agents are non-specific in their distribution and enhancement (Cacheris et al., 1990; Saeed et al., 2000). Just as histologists rely on an arsenal of stains to identify cells under a microscope, our goal is to develop target-specific MR contrast agents whose concentration would be proportional to substrate density.

Here we report work on luxol fast blue MBSN (LFB), a traditional histological stain for myelin first used more than 50 years ago (Klüver and Barrera, 1953). We have introduced a novel role for LFB as a contrast agent for MR imaging. LFB binds to myelinated axons throughout the central nervous system. The molecular structure of LFB, shown in Fig. 1, contains a paramagnetic copper core whose unpaired electrons contribute to local magnetic fields, increasing proton relaxation rates. The goal of this work is to test the hypothesis that in regions where the contrast agent binds, the proton relaxation enhancement will be especially pronounced.

Klüver's earlier work on porphyrins, natural constituents of the white matter of vertebrates, coupled with the knowledge that porphin derivatives bind porphyrins (Klüver, 1944), prompted him to select LFB, a phthalocyanine with a structural appearance similar to porphyrin, as a potential myelin stain (Klüver and Barrera, 1953). Later work by Pearse (1955) showed copper phthalocyanine dyes to stain many myelin constituents, especially lecithin (phophatidylcholine) and sphingomyelin, but also cephalin (phophatidyl-ethanolamine), and cerebroside.

The precise binding site of copper phthalocyanines to myelin remains unknown, but many potential substrates have been

* Corresponding author. 149 13th Street, Charlestown, MA 02129, USA. Fax: +1 617 726 7422.
E-mail address: mlb@nmr.mgh.harvard.edu (M.L. Blackwell).

1053-8119/$ – see front matter © 2009 Elsevier Inc. All rights reserved.
doi:10.1016/j.neuroimage.2009.01.030

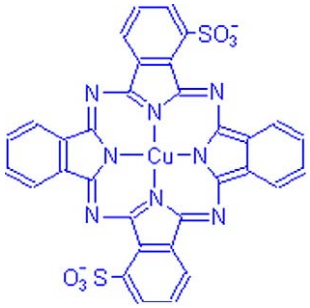

Fig. 1. Chemical structure of luxol fast blue (LFB), an amine salt of a sulphonated copper phthalocyanine (Horobin, 2002). Arrows represent dative bonds between copper and nitrogen atoms.

suggested, including phospholipids (Klüver, 1944; Salthouse, 1962), neurokeratin and proteolipid proteins (Koenig, 1959), and lipoproteins (Scholtz, 1977). In these proposed acid–base interactions, the base of the substrate replaces the base of the dye.

Selectively staining myelin in the human brain enhances the appearance of what neuroanatomist W. J. H. Nauta called the "neocortical warp and woof," or the superposition of radial and tangential organizations of neocortical axons (Nauta and Freitag, 1986). The patterns of these fiber connections, as well as the thickness, prominence, and composition of the six layers of neocortex serve as a metric for dividing the brain into cytoarchitecturally uniform areas. The most widely-used parcellations of neocortex are maps delineating regions based on differences in neuronal density (Brodmann, 1909; Vogt and Vogt, 1942) or myelination (von Economo and Koskinas, 1925). A series of maps based on lipofuscin density (Braak, 1976) present an additional subdivision of areas.

All maps illustrate that function follows form in the neocortex, and regions of the brain involved in processing primary sensory information possess a more distinct pattern of myelination and cellular packing (specifically of granule cells) than dysgranular cortex or agranular cortex, where layer IV is poorly developed or absent. Layer IV is most distinctive in the primary visual area (Brodmann area 17), where it contains a prominent group of tangential fibers called the line of Gennari, after Francesco Gennari, the Italian medical student who discovered this signature mark of primary visual cortex in 1776 (Nauta and Freitag, 1986). This axon plexus is a cell-poor band that divides two sublayers rich in granule cells. In the neighboring regions of primary visual area, these striations merge and the line of Gennari vanishes.

The appearance of layer IV, which varies widely throughout the neocortex, is thus a hallmark of the cortical region in which it resides. As such, we have chosen the visual cortex, and specifically the primary visual area, as a testing ground for our myelin-specific contrast agent. LFB holds great potential as an MR contrast agent for use in imaging with a dual role in correlating MR images with histology.

Materials and methods

Relaxivity of LFB in solution

We measured the longitudinal and transverse molar relaxivities for LFB in ethanol solution as well as in aqueous solution, which was assumed to be more similar to the tissue environment after staining and differentiating with aqueous lithium carbonate (LiCO). Four concentrations of LFB were prepared by modifying a standard histological protocol (Kiernan, 1999). Solvent blue 38 powder (Acros Organics, Morris Plains, NJ) was added to a 20:1 mixture of 95% ethanol and 10% acetic acid. The standard protocol suggests preparation of a 0.1% w/v LFB solution. We increased the concentration of LFB until saturation was reached at approximately 1% w/v. The LFB solution was heated at 56 °C for 24 h, filtered with 90 μm filter paper, and diluted to form three additional concentrations of 2.13, 1.42, and 0.62 mM. These concentrations were later verified using inductively-coupled plasma atomic emission spectrophotometric (ICP-AES) techniques (Jarvis, 1992) by quantifying the amount of copper in each sample.

It was unexpected that LFB would be substantially soluble in water, as only a slight solubility is documented (Horobin, 2002). We were able to produce a 0.12% w/v solution of aqueous LFB by heating the mixture in a 56 °C water bath before filtration. Later measurements after filtering determined a concentration of 0.33 mM. Three aqueous dilutions of 0.25, 0.17, and 0.08 mM were also created and validated with ICP-AES.

Four 3 mm NMR tubes, each filled with a different concentration of LFB, were positioned in a custom-made holder and scanned simultaneously using a 20-mm birdcage coil in a vertical 89-mm bore 14 T magnet (Magnex Scientific, Oxford, England) with a 100 G/cm gradient coil. Susceptibility matching was improved by filling the tube-shaped holder with deionized, distilled water. Scans were repeated in a horizontal 33-cm bore 4.7 T magnet (Magnex Scientific, Oxford, England) with a 40 G/cm gradient coil using a 72-mm birdcage coil. An inversion-recovery prepared spin echo sequence was used to deduce longitudinal relaxation times (TR/TE/TI = 5000/7.5/6–5000 ms at 14 T and 2000/5.2/9–2000 ms at 4.7T; 15 inversion times), and a multi-echo spin echo sequence for the transverse relaxation times (TR/TE = 1000/10–60 ms at both 14 and 4.7 T; eight echos).

Regions of interest (ROIs) were drawn in the central area in each tube; means and standard deviations were plotted against TI or TE. Data were fit to solutions of the Bloch equation for inversion-recovery or spin echo sequences using the Levenberg–Marquardt method, and T1 and T2 were determined, respectively, for each sample. Relaxivities were then estimated by performing linear regression using the concentration relationship:

$$\frac{1}{T_i} = \frac{1}{T_{i_o}} + r_i[\mathrm{LFB}] \tag{1}$$

(Bloembergen et al., 1948), where $i = 1$ for longitudinal relaxation and $i = 2$ for transverse relaxation, and i_o denotes a relaxation time in the absence of contrast agent. Monte Carlo simulations were performed to estimate measurement uncertainty (Press et al., 1988). Zero mean, unit variance pseudorandom numbers were generated, transformed to have the same statistics as the measured data, and propagated through the fitting routine. This procedure was repeated 1000 times, and standard deviations of the resulting relaxivities computed.

Relaxation rates of ex vivo tissue

Samples of visual cortex were obtained from four human brains in which the following criteria were met: 1) unrestricted permission for autopsy had been given; 2) no clinical suspicion of neurologic disease; 3) no clinical evidence of blood borne pathogens, including HIV, hepatitis, or prion disease; and 4) gross examination of the brain at the time of removal did not indicate the presence of previously unsuspected pathology. Mean age of samples was 55 years; two males and two females were used. The brain tissue was fixed in formalin for more than eleven weeks, which is the minimum time required for transverse and longitudinal relaxation rates to reach equilibrium (Tovi and Ericsson, 1992; Blamire et al., 1999).

The timing for the previous stages was determined heuristically, as described in subsequent sections. Blocks of tissue were immersed in a phial containing 1% LFB solution, placed in a water bath, and removed after a minimum duration had elapsed, specifically 24 h per 0.7 mm thickness. Next, samples were blotted to remove excess LFB, rinsed for

Table 1
Longitudinal relaxivities of luxol fast blue (LFB) in ethanol-based or aqueous solutions, at 4.7 and 14 T field strengths

Preparation	Field strength (T)	R1 (s^{-1}/mM)
LFB in EtOH	4.7	0.15 ± 0.01
Aqueous LFB	4.7	0.09 ± 0.02
LFB in EtOH	14	0.12 ± 0.01
Aqueous LFB	14	0.09 ± 0.04

5 min each in 95% ethanol and doubly-distilled water (Millipore, Billerica, MA). Samples were immersed in an 0.05% lithium carbonate solution (Sigma-Aldrich, St. Louis, MO) at room temperature for 400 min to achieve optimal differentiation.

Blocks of tissue, approximately $3 \times 1 \times 1$ cm^3, were removed from samples along the calcarine sulcus. Each tissue sample was processed in three subsequent manners and imaged after each preparation: 1) formalin treatment only, 2) *en bloc* staining protocol, using an ethanol-acetic acid solvent containing no LFB, and 3) *en bloc* staining protocol using 1% LFB.

Ex vivo sample preparation

Lateral diffusion is the only available transport mechanism for LFB through fixed tissue. Histological protocols for tissue samples 20–50 μm in thickness suggest using immersion times between 18 and 24 h at room temperature (Kiernan, 1999). We wish to scale these durations to stain larger sections, lobes, hemispheres, or even the entire brain. The diffusion rate of LFB in fixed tissue has not been reported previously; our initial observations suggested a slow rate that may prohibit staining very large samples *en bloc*. We sought to accelerate LFB penetration by placing phials containing LFB and tissue samples into a hot water bath maintained at 56 °C, modeled after an optimized protocol that stained thin tissue slices at this temperature (Geisler et al., 2002). To determine the necessary incubation duration, $1 \times 1 \times 3$ cm^3 tissue blocks of parietal cortex from the same formalin-fixed brain were immersed in a 1% LFB solution, kept at room temperature, and removed, bisected, and photographed at 6-hour intervals. Similar tissue blocks were also immersed in a phial of LFB, which was then placed in a hot water bath kept at 56 °C. These 56 °C samples were also removed, bisected, and photographed at 6-hour intervals for comparison.

Methods used to differentiate the LFB-stained tissue were based on a standard histological protocol (Kiernan, 1999), with immersion times adjusted systematically to achieve a duration that would sufficiently remove unbound LFB from the gray matter without over-differentiating white matter. Tissues were immersed in an 0.05% w/v aqueous solution of lithium carbonate at room temperature for durations between 4 and 570 min. After each interval, samples were removed from solution, blotted, photographed, and returned to solution.

High-resolution MR imaging

Prior to imaging, *ex vivo* tissue samples were immersed in a proton signal-free perfluoropolyether (Fomblin, Solvay Solexis, Thorofare, NJ) in a low-pressure environment. This procedure was performed to remove artifact-inducing air bubbles within the tissue; preliminary experiments determined a duration of 24 h at room temperature was sufficient to eliminate a majority of air bubbles. Tissue blocks were wedged between two polyethylene caps (Wilmad Lab-Glass, Buena, NJ) to prevent motion.

Magnetic resonance imaging was performed at 14 T using a 10-mm diameter birdcage coil and at 4.7 T with a 72-mm diameter birdcage coil. As described earlier, inversion-recovery prepared spin echo sequences were used for T1 mapping and multi-echo spin echo sequences for T2 mapping. These acquisitions were three-dimensional with an isotropic resolution of 150 μm.

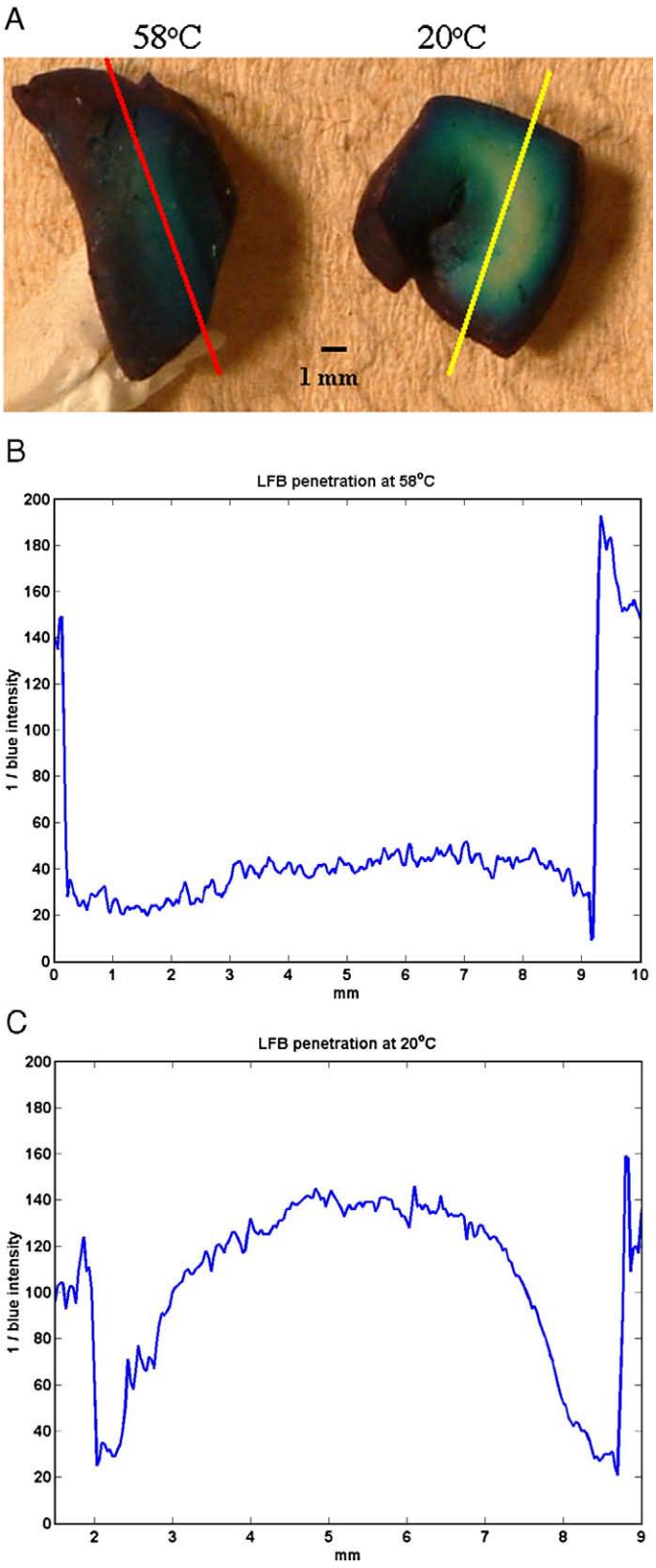

Fig. 2. (A) Two representative samples of human brain tissue, immersed in luxol fast blue (LFB) at either 56 °C (left) or 22 °C (right) for 24 h and then bisected. Plotted below for each sample is the reciprocal of the blue intensity along a path perpendicular to the surface. LFB was found to have a penetration rate of 1.4 mm per day at the warmer temperature (B), compared to 0.5 mm per day at the cooler temperature (C).

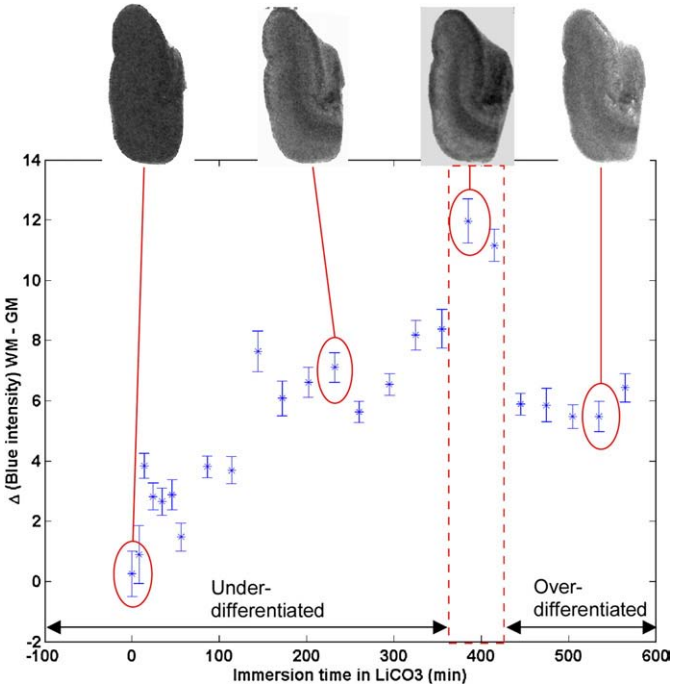

Fig. 3. Samples of LFB-stained human brain tissue were immersed in a 0.05% aqueous solution of lithium carbonate (LiCO) for intervals ranging between 0 and 520 min, blotted, and photographed. Plotted above is the blue intensity difference between white matter (WM) and gray matter (GM) as a function of immersion time. Representative images appear for four time points.

Regions of interest were drawn to encompass outer gray matter (GMo, representing layers I–IVa), inner gray matter (GMi, representing layers IVc–VI), white matter, and background regions. Care was taken to avoid edges or artifacts, and classification of ROIs was later validated by aligning histological sections to MR images. Means and standard deviations of ROIs were plotted against TI or TE. Data were fit to solutions of the Bloch equation for inversion-recovery or spin echo sequences using the Levenberg–Marquardt method, and T1 and T2 were determined, respectively, for each ROI in each sample preparation. A paired, two-tailed Student's *t*-test assessed the significance of numerical differences in relaxation rates arising from staining tissues with LFB. Differences were considered significant if $p<0.05$.

Next, calculated relaxation rates were used to determine sequence parameters that maximize contrast per unit time (i.e., the square-root of TR) for both T_1- and T_2-weighted imaging sequences. Solutions of the Bloch equations were used for an inversion-prepared spin echo sequence to achieve T1 weighting, selecting inversion times for each preparation equal to the mean T1 of WM, GMi, and GMo ROIs. A linear search of contrast space for a given inversion time was used to select the repetition time for each preparation that maximized the root mean squared (RMS) contrast at each field strength, defined as:

$$\mathrm{CNR}_{\mathrm{RMS}} = \sqrt{\frac{1}{n}\sum_{i,j}^{n} \frac{\left(\mathrm{SNR}_i - \mathrm{SNR}_j\right)^2}{\sigma_{\mathrm{bg}}}} \tag{2}$$

where SNR_i and SNR_j are the signal-to-noise ratios for adjacent regions i and j, respectively, for n such adjacent regions, and σ_{bg} is the standard deviation of the background signal. Many studies have analyzed differences in MR images using RMS difference methods (Pisani et al., 2004; Shattuck et al., 2001). For T2 weighting, a spin echo sequence was used, selecting an echo time for each preparation equal to the mean T2 of WM, GMi, and GMo ROIs. Similarly, a linear search of contrast space was used to determine the repetition time and flip angle that maximized the RMS contrast for each preparation and field strength. Finally, images were acquired at both field strengths using the determined parameters for maximal contrast, and the RMS CNR was computed for each sample preparation.

In addition, three 80-micron isotropic MR images of formalin-, ethanol-, and LFB-prepared samples were acquired at 14 T with intermediate weightings. The following sequences were used for each sample: spin-echo (TR/TE = 2000/20.5 ms, NEX = 8), gradient-echo (TR/TE = 200/22.7 ms, Θ = 30°, NEX = 8), and inversion-prepared spin echo (TR/TE/TI = 5000/7.2/300 ms, NEX = 8). Gradient echo acquisitions were chosen because the minimum TR and TE were lower than that of spin echo sequences, yielding greater SNR. Acquisition bandwidths and readout gradient directions were identical for these sequences. Averages of signal intensity along 12 profiles perpendicular to the cortical surface were calculated in the same region of each image to investigate laminar characteristics.

To help identify lamina in MR images of LFB-stained samples, a similar profile analysis was conducted on an image of Astrablau-stained

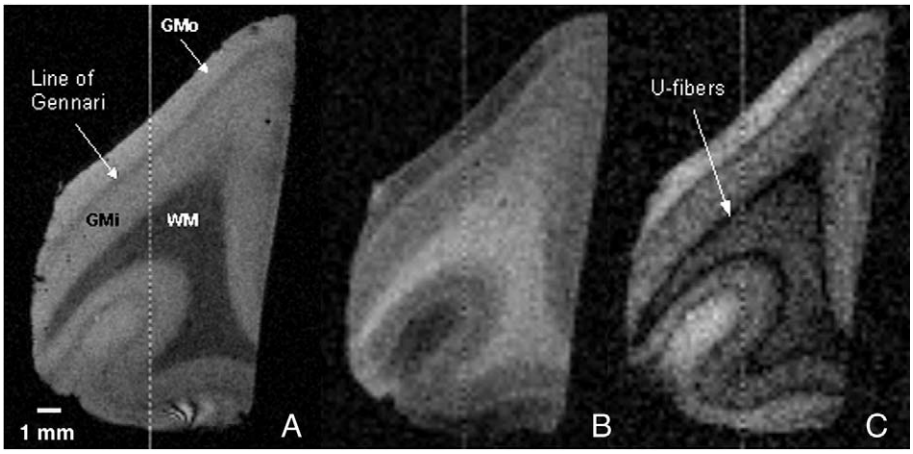

Fig. 4. MR images with T2-weighting (A), T1-weighting (B), and intermediate weighting at 14 T of an LFB-stained, LiCO-differentiated sample of human visual cortex. Three regions of interest used for analysis are clearly visible in all images: white matter (WM), inner gray matter (GMi), comprised of layers IVc–VI, and outer gray matter (GMo), comprised of layers I–IVa. The Line of Gennari, layer IVb that is heavily myelinated in visual cortex, is also prominently displayed. In image C, the subarcuate fibers, or "u-fibers," are also resolvable and appear darker than the underlying white matter. Images have 150-micron isotropic resolution and were acquired using (A) a gradient echo sequence (TR/TE = 80/15.2 ms, Θ = 30°); (B) an inversion-prepared spin echo sequence (TR/TE/TI = 5000/5.96/320 ms); and (C) an inversion-prepared spin echo sequence (TR/TE/TI = 5000/5.96/120 ms).

human striate cortex as found in Braak (1976). This was considered an appropriate comparison, as Braak's sample was large for histological analysis (800 μm in thickness) and was subjected to a similar *en bloc* preparation. Furthermore, Astrablau, the dye used to stain lipofuscin inclusions, is a copper phthalocyanine dye (Bloom and Kelly, 1960) with a structure similar to LFB.

Validation of LFB distribution and concentration

After MR imaging was completed, two samples were sectioned into 40-micron slices with a freezing microtome. Sections were mounted on glass slides, dehydrated in progressive ethanol concentrations, cleared in xylene, and coverslipped. No additional myelin stains were added to the sectioned slices, and one sample was counterstained with a 0.1% w/v solution of cresyl violet, following a standard protocol (Kiernan, 1999). Bright-field microscopy was performed using a Nikon Eclipse 50i microscope. Images were collected using a charge-coupled device camera (Photometrics, Tuscon, AZ) and analyzed with SPOT 4.0 Advanced Version Software (Diagnostic Instruments, Sterling Heights, MI). Additional infrared images having 21-micron in-plane resolution were obtained with the LI-COR Odyssey (Lincoln, NE) to aid registration between MR and histological images using normalized mutual information (Amira, ZIB, Berlin).

Inductively-coupled plasma atomic emission spectrophotometric (ICP-AES) techniques (Jarvis, 1992) were employed to determine the concentration of LFB in tissue samples by quantifying the amount of copper in each sample. Prior to measurement, the 1% LFB solution was diluted by 100×, and a reference sample of 20:1 ethanol–acetic acid was prepared to ascertain matrix effects. For tissue measurements, LFB-stained, LiCO-differentiated samples were segmented into regions of white matter or gray matter, based on optical density. Tissue segments of white matter, weighing 50.2 mg, and gray matter,

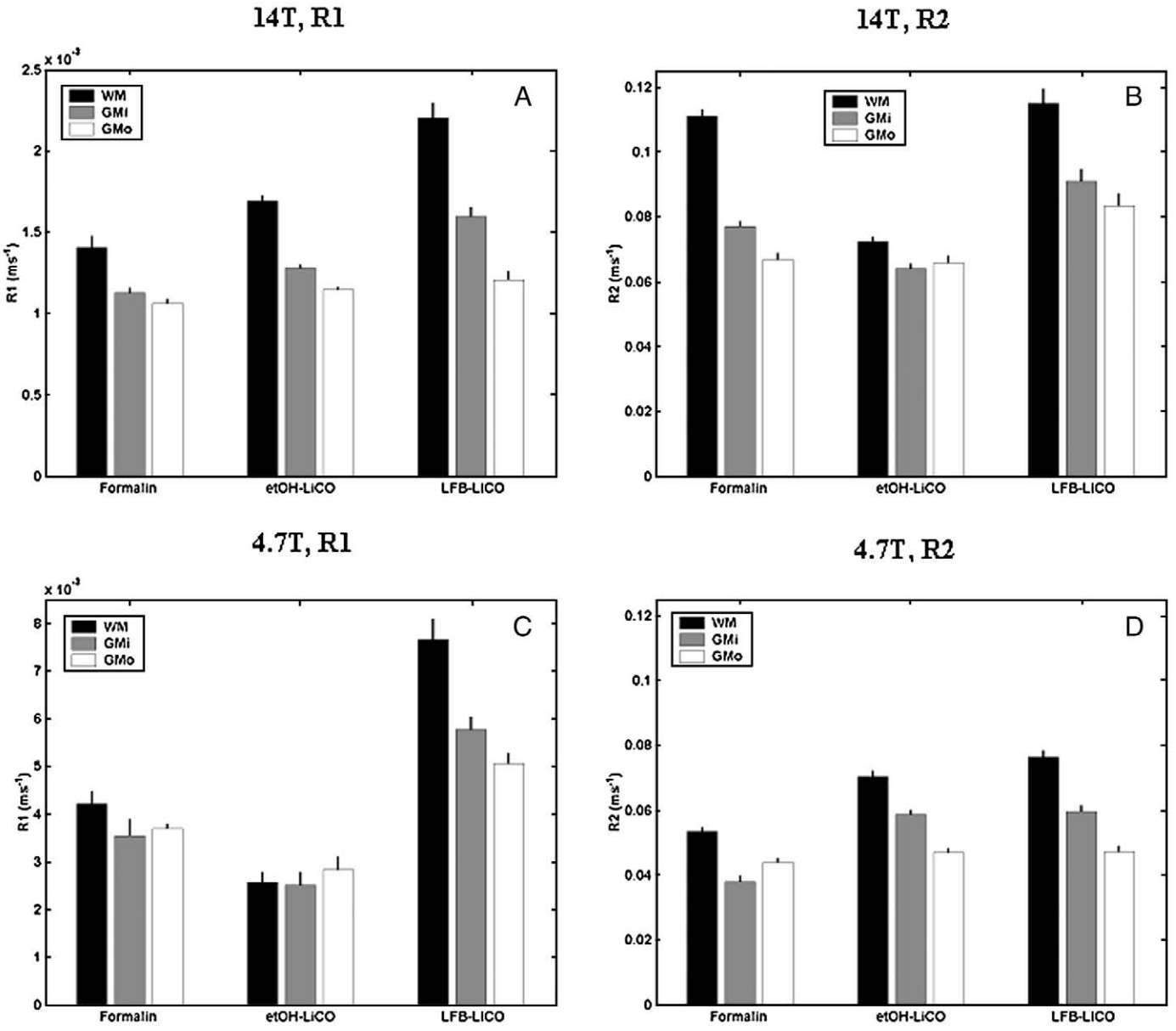

Fig. 5. Comparison of relaxation rates in white matter (WM), inner gray matter (GMi), and outer gray matter (GMo) for three differing preparations of fixed human tissue samples: 1) formalin alone, 2) 95% ethanol immersion and 0.05% lithium carbonate differentiation, or 3) LFB immersion and 0.05% lithium carbonate differentiation. (A) At 14 T, R1 increased significantly ($p<0.05$) for all ROIs (WM, GMi, and GMo) for all comparisons (formalin–EtOH, formalin–LFB, and EtOH–LFB). (B) At 14 T, R2 increased significantly for all ROIs and all comparisons except GMo between formalin and EtOH preparations. (C) At 4.7 T, R1 increased significantly for all ROIs and all comparisons. (D) At 4.7 T, R2 increased significantly for all ROIs and all comparisons except GMi and GMo between EtOH and LFB preparations.

weighing 44.5 mg, were digested in two separate phials containing 2 mL of a 1:1 mixture of 100% nitric acid and 100% sulfuric acid. After 48 h, all tissue fragments had been fully digested, and each solution was diluted with Triton-X (Sigma-Aldrich, St. Louis, MO) to a final volume of 20 mL. A reference sample of the nitric–sulfuric–Triton solution was prepared to estimate matrix effects.

Measured tissue concentration of LFB was then compared to measured solution concentration to compute partition coefficients for gray matter and white matter, following the method of Kety (1951).

Results

Relaxivity of LFB in solution

Longitudinal and transverse relaxation rates of LFB in solution increased linearly with LFB concentration; calculated longitudinal relaxivities for LFB in ethanol solution or aqueous solution are displayed in Table 1. As expected, longitudinal relaxivity was greater at lower field strength and transverse relaxivity increased with field strength. These longitudinal relaxivities are consistent with literature values for longitudinal relaxivities of chelated copper compounds at 1.5 T, which range from 0.12 to 0.21 s^{-1}/mM (Lauffer, 1987). The measured longitudinal relaxivities of aqueous LFB were lower than those for ethanol-based LFB at both 4.7 and 14 T.

Ex vivo sample preparation

Shown in Fig. 2 are images (A) and intensity profiles (B, C) through two representative, bisected samples of visual cortex that had been incubated in LFB for 24 h. From a series of profiles, the estimated rate of penetration of LFB through samples was 0.5 ± 0.03 mm/day at room temperature and 1.4 ± 0.03 mm/day at 56 °C.

Subsequent treatment of samples with 95% ethanol removed additional LFB dye from the tissue surface. A five-minute immersion interval was found to be sufficient, regardless of tissue size, as longer durations did not result in further visually remarkable decreases in dye density from the tissue surface. Rinsing tissues in doubly-distilled water removed slightly more LFB, as noted from the resulting blue tint of the liquid. Immersion times exceeding 5 min did not appear to remove any additional dye from the tissue.

Representative images of samples before and after LiCO treatment appear in the top of Fig. 3. After the initial immersion in LFB, samples appear a uniform blue with white matter having a slightly darker color. Following treatment with LiCO, gray matter becomes lighter in appearance as LFB is removed, while white matter retains its darker blue hue. The contrast between white and gray matter is plotted as a function of differentiation time in Fig. 3. An immersion time of 400 min per centimeter thickness of the sample was deemed sufficient for the lithium carbonate solution to fully penetrate the sample without over-differentiating the more superficial lamina.

High-resolution MR imaging

Three MR images acquired at 14 T of an LFB-stained, LiCO-differentiated sample of human visual cortex appear in Fig. 4. Four distinct regions are apparent in the T2*-weighted image (Fig. 4A) and the T1-weighted image (Fig. 4B); these areas resemble lamina, stratifying into parallel bands of differing thickness, and follow the convolutions of the lingual gyrus. The innermost area is white matter (WM); the more superficial, thick band is the heavily-myelinated layer IVb, also known as the line of Gennari. Placed between the white matter and layer IVb are layers IVc through VI, collectively referred to in this paper as inner gray matter (GMi). There is no consensus in the literature concerning the specific subdivisions for this area, and the nomenclature varies depending upon authors and histological techniques used (see Plate 9 in Braak, 1976, for comparison of 11 metrics of subdivision.)

The outermost region encompasses layers I through IVa and is called here the outer gray matter (GMo). An additional dark band is discernable in the intermediate-weighted image (Fig. 4C), separating the WM and GMi. This is a layer of u-fibers, especially prominent in visual cortex.

Longitudinal and transverse relaxation rates were calculated in these three regions of interest (ROIs) for MR acquisitions of samples prepared successively with formalin, ethanol, and LFB at 4.7 and 14 T. As seen in Fig. 5, at both field strengths, LFB was more effective in increasing longitudinal relaxation rates in all ROIs than either the formalin or ethanol preparation. At 4.7 T, the percentage increase in R1 for the LFB samples compared to the ethanol preparation was 199% for WM, 129% for GMi, and 78% for GMo. At 14 T, the percentage increases in R1 were more modest than at the lower field strength and equaled 30% for WM, 25% for GMi, and 5% for GMo. All changes were statistically significant ($p<0.05$) and suggest LFB effected an increase in R1 proportional to myelination.

LFB was also more effective in increasing transverse relaxation rates in all ROIs than either formalin or ethanol preparation at both field strengths. However, as expected due to a higher baseline rate, the increase in R2 effected by LFB was a much smaller percentage change than that observed in R1. At 4.7 T, the percentage increase in R2 for the LFB samples compared to the ethanol preparation was 8.4% for WM, 1.3% for GMi, and 0.5% for GMo. At 14 T, R2 increased by 59% for WM, 42% for GMi, and 27% for GMo. The changes seen at higher field are larger in part because of the increased field strength but could also result from rehydration effects, which lower R2 values in the ethanol-prepared, LiCO-differentiated sample compared to the sample treated with formalin only.

The root mean squared (RMS) contrast between adjacent regions, per unit time, for formalin-, ethanol-, and LFB-treated samples at 4.7 and 14 T are displayed in Table 2. These values were obtained via simulations of the Bloch equations for T1- or T2-weighted sequences, as explained in the previous section. The LFB preparation has the largest contrast per unit time for T1- and T2-weighted imaging at 4.7 T, although the propagated error from the fitted parameters reduces the significance of the gain in contrast. At 14 T, signal differences are larger, and the LFB preparation produces a highly significant increase in contrast for T1-weighted imaging. However, the LFB did not enhance T2 contrast compared to the formalin preparation.

Experimental values of contrast per unit time for each preparation, (Table 2) confirm the simulation predictions for contrast: LFB effects a significant increase in T1 laminar contrast per unit time at both field strengths but does not significantly increase T2 contrast above that of controls. The improvement in laminar contrast can be seen in the T1-weighted images of visual cortex prepared with ethanol or LFB, displayed in Fig. 6. It is difficult to obtain T1 contrast

Table 2
Comparison of contrast-to-noise ratios per unit time for control and LFB-treated samples in T1- and T2-weighted images

Preparation	Image weighting	Field strength (T)	Theoretical CNR/time	Experimental CNR/time
Control	T1	4.7	46.7 ± 11.1	11.4 ± 8.1
LFB	T1	4.7	75.3 ± 8.7	37.4 ± 9.2
Control	T2	4.7	92.1 ± 18.8	77.9 ± 1.8
LFB	T2	4.7	101.0 ± 9.6	84.7 ± 8.9
Control	T1	14	152.6 ± 35.1	36.3 ± 5.3
LFB	T1	14	410.2 ± 25.4	134.0 ± 6.7
Control	T2	14	322.8 ± 16.9	146.6 ± 19.4
LFB	T2	14	375.0 ± 11.2	140.0 ± 30.4

Control samples for T1 measurements were treated with ethanol and for T2 measurements, formalin. CNR values were calculated at 4.7 and 14 T field strengths both theoretically, based on measured relaxation times, and experimentally, using scan parameters predicted to maximize contrast (listed in Figs. 6 and 7, respectively). Increases in CNR were significant ($p<0.05$) for all comparisons except T2 weighting at 4.7 T (theoretical and experimental) and 14 T (experimental only).

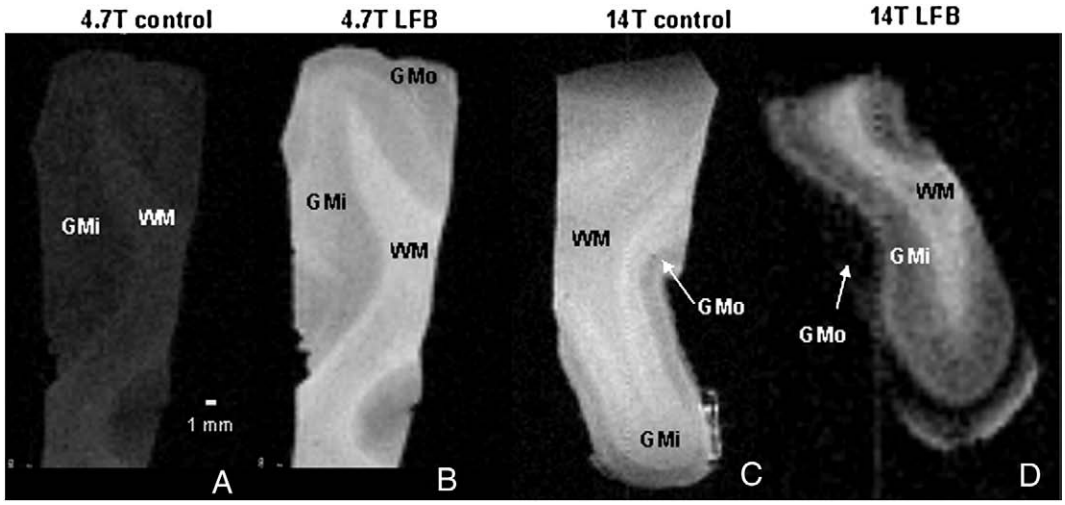

Fig. 6. T1-weighted MR images of tissues "stained" with ethanol and differentiated with lithium carbonate (A,C) exhibit less contrast between adjacent laminar regions, white matter (WM), inner gray matter (GMi), and outer gray matter (GMo) than samples stained with LFB and differentiated with lithium carbonate (B,D). Images were acquired with 150-micron isotropic resolution using an inversion-prepared spin echo sequence with the following parameters (in ms): TR/TI = 800/380.2 (A); 1000/167.4 (B); 3800/749.1 (C); 3500/636.6 (D). Samples A and B were imaged at 4.7 T, samples C and D at 14 T. Eight averages were performed for each scan.

in *ex vivo* samples; in fact, the authors are not aware of any published MR images of *ex vivo* tissue in which white matter appears brighter than gray matter, as typical for *in vivo* T1-weighting. This traditional weighting is achieved more so in the LFB preparations (Figs. 6B and D) than in the ethanol controls (Figs. 6A and C). The brightening of WM aids identification of the WM–GMi boundary at both field strengths. Furthermore, the GMi is more distinct from GMo in the LFB preparations, due in part to the enhanced detection of heavily-myelinated layer IVb, which appears brighter than adjacent lamina at both field strengths. In addition, GMi has a larger signal intensity than GMo at 14 T, presumably because of its increased myelination. Thus, LFB enhances intralaminar contrast on T1-weighted images by increasing the signal intensity in proportion to myelination.

Differences in laminar contrast can also be seen between T2-weighted images of visual cortex prepared with formalin or LFB (Fig. 7). WM and GMi regions appear slightly darker in the LFB-treated samples (Figs. 7B and D) than in the formalin controls (Figs. 7A and C). At 4.7 T, LFB darkens the appearance of GMi, which enhances the GMi–GMo transition but blurs the boundary between WM and GMi. At 14 T, there are marked differences in the appearance of GMi in the control and LFB data sets. In the control image, GMi is fairly homogenous, with a slightly larger signal intensity near the fundus of the gyrus. However, in the LFB sample, the uniformity of GMi is interrupted by fine lines having perpendicular orientation to the laminae.

These fine lines could be interpreted as blood vessels or radial fascicles, which are fine, myelinated axons. We conjecture these lines are more likely to be radial fascicles than blood vessels for two reasons: LFB-specificity and location/orientation. These lines are more prominent in the LFB-treated sample than in the non-LFB sample. Accumulation of contrast agent along these radial fibers could contribute to compartmental susceptibility effects, resulting in the stippled appearance of the more myelinated, inner layers in the MR images of LFB-prepared samples. LFB has no known specificity for blood vessels, which are found both in gray and white matter; therefore, it is unlikely that LFB is binding to the vessels. Radial fascicles extend from the white matter to layer III in slender bundles (Nauta and Freitag, 1986) and have been documented to be present in higher density and greater thickness in mammalian visual cortex

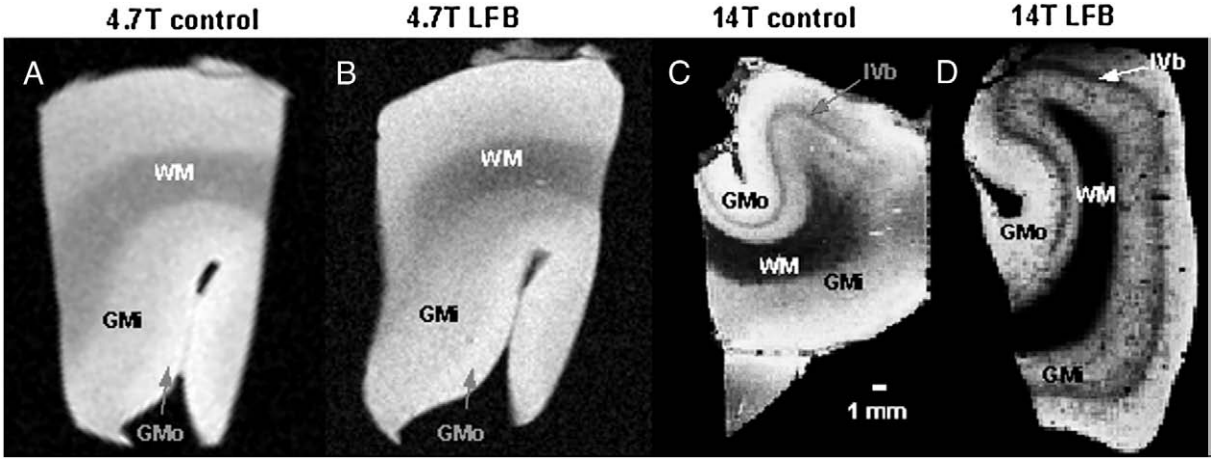

Fig. 7. T2-weighted MR images of control tissues treated with formalin only (A, C) compared to tissues stained with LFB and differentiated with lithium carbonate (B, D). Samples A and B were imaged at 4.7 T, samples C and D at 14 T. White matter (WM) and inner gray matter (GMi) appear darker in LFB-treated samples, which, at 4.7 T, enhances the transition between GMi and outer gray matter (GMo) but blurs the WM-GMi boundary. In addition, at 14 T, the GMi in the LFB sample has a stippled appearance, presumably due to compartmental susceptibility effects caused by accumulation of contrast agent along radial fibers. Images were acquired with 150-μm isotropic resolution using a spin echo sequence, choosing the following parameters: TR(ms)/TE(ms)/Θ: 60/22.5/45° (A); 60/17/45° (B); 100/12.3/20° (C); 100/10.6/20° (D) Eight averages were performed for each scan.

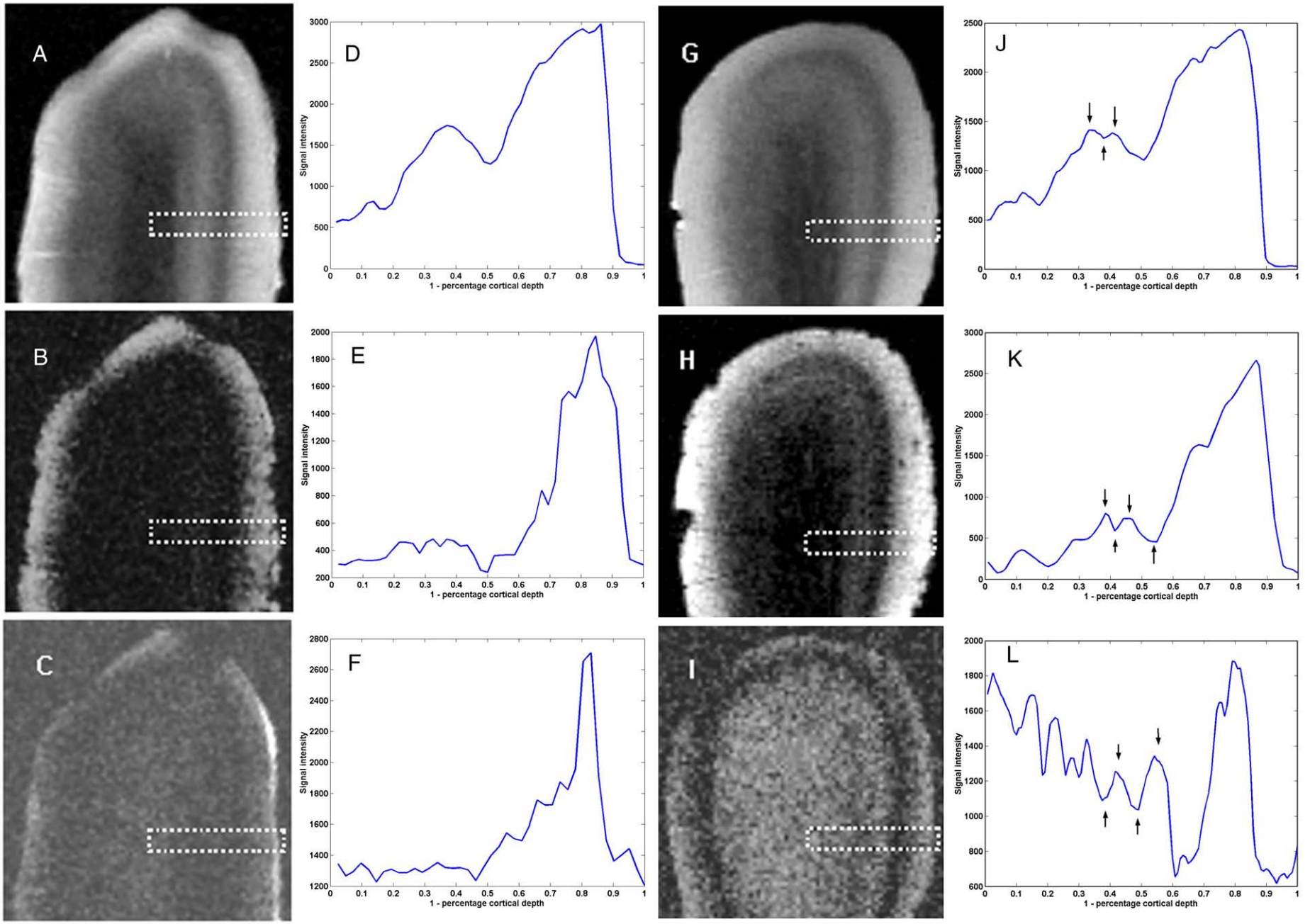

Fig. 8. Three separate, 80-micron isotropic resolution MR acquisitions at 14 T of ethanol control samples (A–C) and LFB-stained preparations (G–I). Images A and G are spin-echo acquisitions (TR/TE = 2000/20.5 ms, NEX = 8), images B and H, gradient-echo acquisitions (TR/TE = 200/22.7 ms, Θ = 30°, NEX = 8), and images C and I, inversion-prepared spin echo acquisitions (TR/TE/TI = 5000/7.2/300 ms, NEX = 8). (D–F, J–L) Averages of signal intensity along 12 profiles perpendicular to the cortical surface were calculated in the region illustrated by the dotted rectangle and are plotted to the right of each image. Additional lamina that become resolvable in the LFB preparations are highlighted with arrows (J–L).

(Ungerleider and Desimone, 1986; Innocenti et al., 2002). The fine lines in the MR images appear to stop in the more superficial cortical layers, just beyond the Line of Gennari, which is consistent with the known distribution of radial fascicles. Vessels in the brain are reported to be isotropically-oriented in occipital cortex (Manoonkitiwongsa et al., 2001) and the authors are not aware of studies showing a greater vascular density in layers III–VI. The identity of these fine lines can be ascertained with more certainty by correlating MR and histological images of identical samples; this research is in progress.

In the high-resolution images, additional laminar structure becomes apparent in the LFB-treated sample that are not resolvable in control data (Fig. 8). Two structures were considered resolvable according to the Rayleigh criterion if two peaks are separated by a minimum having a height no more than 75% of the smaller peak height (Lord Rayleigh, 1874). Images of the ethanol-treated control sample reveal some laminar structure (Figs. 8A–C). A laminar profile perpendicular to the cortical surface of the spin echo acquisition is plotted in Fig. 8D. A dip in signal intensity (73% of peak height) corresponds to layer IVb. This is the only feature resolvable according to the Rayleigh criterion. A broad local maxima appears for subjacent layers and no additional subdivisions can be made. In the profile through the gradient echo image (Fig. 8E), a narrow dip appears in the location of layer IVb as well as a small peak that could correspond to a more superficial layer. A profile through the more T1-weighted image (Fig. 8F) reveals a series of shallow peaks and troughs that could correspond to additional lamina, all superficial to layer IVb.

Profiles through all acquisitions of the LFB-treated sample (Figs. 8J–L) reveal peaks and troughs corresponding to four distinct lamina. Arrows have been added to emphasize lamina on the LFB profiles that cannot be distinguished in the control profiles. These additional layers are inferior to the prominent line of Gennari, and alternate in signal intensity compared to the myelinated layer IVb. Specifically, in the T2-weighted spin echo and T2*-weighted gradient echo acquisitions (Figs. 8G and 8H, respectively), layer IVb appears as a dark stripe and two fine, brighter lines are discernable, separated by a thin, darker layer. In the laminar profiles, the layers appear as a series of peaks and troughs, and are more resolvable in the profile derived from the gradient-echo image (dip-to-peak height ratios of 73%, 80%, and 62%, respectively). In the more T1-weighted image (Fig. 8I), there is a lower contrast-to-noise ratio overall, but the averaged profile reveals local maxima and minima at the same locations as in the other acquisitions, but with a reversal in polarity. Specifically, layer IVb now appears as a local maxima, the next layer as a dip, the next as a peak, and the last as a dip (dip-to-peak height ratios of 87%, 82%, and 77%, respectively). These additional layers follow the course of the line of Gennari, ending abruptly at the V1–V2 transition, as can best be seen in Fig. 8H.

A similar profile analysis was performed on an Astrablau-stained image of striate cortex (Fig. 9A, modified from Braak, 1976). In this inverted image, signal intensity is proportional to lipofuscin density. The peaks and dips appearing in a profile through (Fig. 9B) could be identified from the labels on the original image. Progressing from superficial to deep layers, the first, wide dip is unlabeled, but has the proper thickness and location to be layer IVb. The next peak is consistent with layer IVcb; the next trough, layer IVd, and the final peak, Va. None of the additional listed layers (Vb–VIb) could be distinguished.

There is a remarkable resemblance between the profile through the histological preparation and the profile through the gradient echo image of the LFB-prepared sample (Fig. 9C). Expressing the abscissa of each

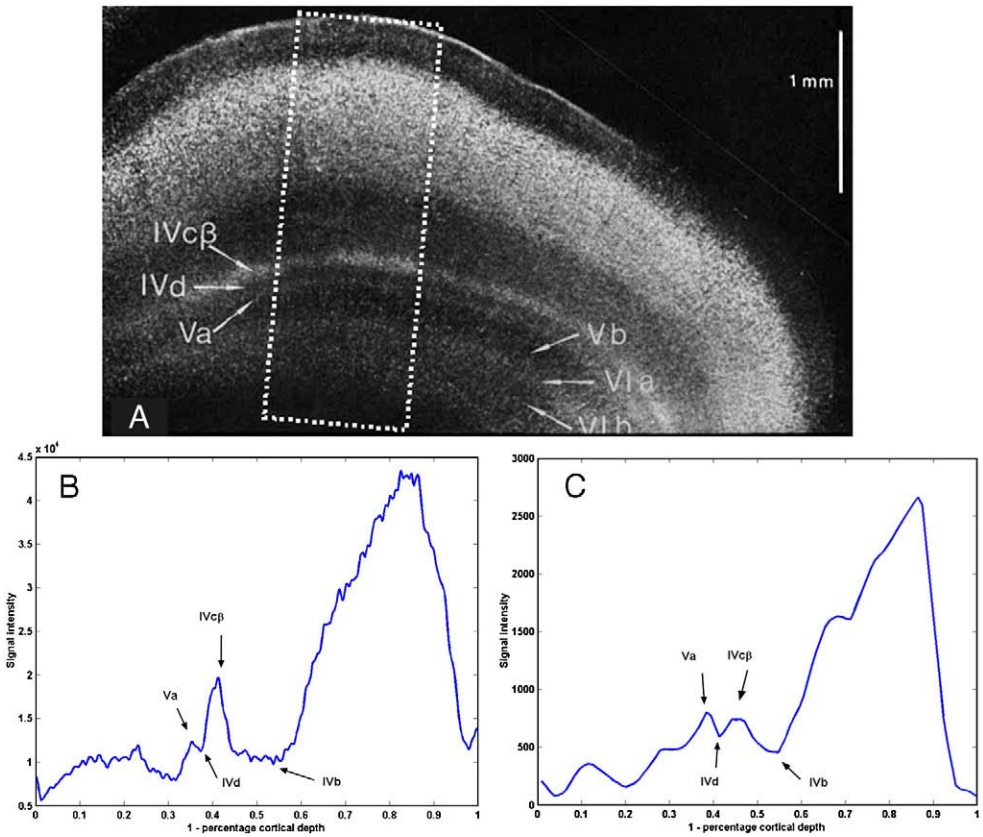

Fig. 9. (A) An inverted light microscope image (Fig. 5, Plate 2 from Braak, 1976) of an 800 micron-thick slab of Astrablau-stained human visual cortex. (B) Average signal intensity along 120 profiles perpendicular to the cortical surface were calculated in the dotted rectangular region shown in (A). Arrows have been added to label the peaks and troughs corresponding to the documented lamina (layers IVb, IVcβ, IVd, and Va) in (A). (C) Fig. 8E is repeated here for comparison: Average of signal intensity along 12 profiles perpendicular to the cortical surface calculated for the rectangular area shown in Fig. 8B.

graph as a percentage of cortical depth helped identify the additional lamina in the high-resolution MR images of LFB-prepared samples.

Validation of LFB distribution and concentration

A high-resolution image acquired at 14 T was matched to an infrared image of 40-micron slice preparation and then to a 2×-magnification light microscope image (Figs. 10A–C). The alignment is not exact due to tissue damage incurred during slice preparation, common in traditional histology. Neither the *en bloc* staining technique nor the perfluorocarbon embedding appear to have altered the microstructural appearance of the fixed tissue. The macroscopic distribution of LFB is similar to standard histologic preparations: the darkest staining areas of visual cortex are the white matter and the heavily myelinated line of Gennari (Fig. 10C). The optical density of the tissue appears proportional to myelin content, and the deeper, more myelinated cortical layers appear darker than the more superficial layers. Upon higher magnification (10×, Fig. 10D), the dense meshwork of subcortical white matter contains many blue fibers. At a microscopic view (40×, Figs. 10E–F) individual radial fibers can be distinguished projecting perpendicular to the cortical lamina, and closer to layer IVb, horizontal fibers can be distinguished that belong to this tangential net.

In Fig. 14, a 40-micron histological image counterstained with thionine is matched to a 150-micron MR image acquired at 14 T. This histological preparation permitted segregation of eight laminar divisions: layers I, II–III, IVa, IVb, IVc, V, VI, and white matter. These lamina confirm our previous choices of regions of interest first introduced in Fig. 5.

The ICP-AES measurements determined 12.63 ± 0.23 μg copper per gram gray matter, or 0.45 ± 0.01 mM, and 26.32 ± 0.28 μg copper per gram white matter, or 0.93 ± 0.01 mM. These are minimal values for the tissue samples, as storage in doubly-distilled water before tissue digestion did cause some contrast agent seepage, as noted by the bluing of the solution. Using these values, the partition coefficient was calculated to be 15.8% for gray matter and 32.7% for white matter.

Discussion

This work has introduced luxol fast blue as a novel magnetic resonance contrast agent with binding affinity for myelinated constituents of the brain. This specificity for lipid constituents resulted in an increase in longitudinal and transverse relaxation rates of tissue dependant on myelination. Relaxation rates of white matter were increased sufficiently to permit T1-weighted images of *ex vivo* samples in which white matter signal is hyperintense to gray matter, similar to T1-weighted *in vivo* imaging. Increased longitudinal relaxation rates can also permit a concomitant decrease in TR, resulting in reduced scan times. This is an important advantage, especially for high-resolution images with very large matrix sizes and lengthy scan times.

Contrast was increased in MR images of LFB-stained *ex vivo* brain tissues prepared using the newly-developed *en bloc* staining technique, especially for T1-weighting, which enhanced delineation between upper lamina (layers I–IVa) and the more myelinated lower lamina (layers IVc–VI). Additional visual cortex sublayers IVca, IVd, and Va were most apparent in T1- and T2*-weighted images of LFB-stained samples, but not discernable in control preparations. These results have not been achieved in other *ex vivo* studies without contrast agents (Tovi and Ericsson, 1992; Benveniste et al., 1999; Fatterpekar et al., 2002; Barbier et al., 2002; Walters et al., 2003; Pfefferbaum et al., 2004; Eickhoff et al., 2005) or studies using gadolinium-based contrast agents (Johnson et al., 2002).

Increased T1 contrast may be explained by dipolar interactions between bound or diffusing molecules and the additional magnetic

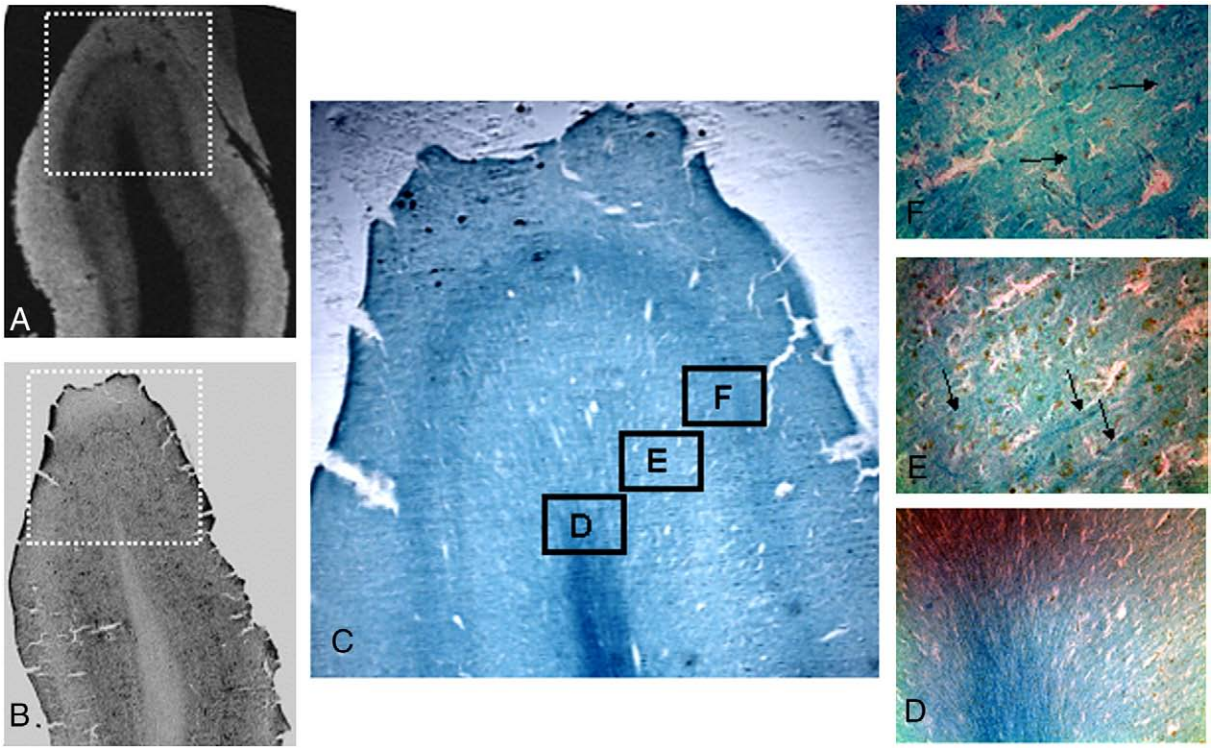

Fig. 10. Distribution of LFB among myelinated fibers for *en bloc* staining mimics that of traditional histologic preparation. (A) Gradient echo acquisition (TR/TE = 60/7.7 ms Θ = 30°) at 14T; 80-micron isotropic resolution. (B) Infrared image obtained to aid alignment of MR and histological images; 21-micron in-plane resolution. Dotted squares in (A) and (B) indicate the approximate location of the 40-micron thick, 2× magnification slice preparation in (C), to which no additional stain has been added. The macroscopic LFB distribution is proportional to myelination and is concentrated in white matter and the line of Gennari, causing these areas to have a darker intensity in light microscopy. Illustrated in (C) are three additional regions of interest: (D) 10× magnification of subcortical white matter; (E) 40× magnification of inner gray matter (GMi) reveals radial fibers (arrows) retaining LFB stain; (F) 40× magnification closer to layer IVb showing tangential fibers (arrows) that retaining LFB stain.

field produced near the paramagnetic centers of the LFB agent (Bloembergen et al., 1948; Lauffer, 1987). These fields provide additional relaxation pathways and highlight cortical sublayers that possess varying degrees of myelination. The observed enhancement of sublayers on gradient echo acquisitions was more surprising. In these images we were able to resolve layers IVca, IVd, and Va, structures that, heretofore, have only been seen in histological preparations. The family of compounds to which LFB belongs is prone to aggregation by van der Waals' attractive forces between phthalocyanine rings (George et al., 1998). Compartmentalization of dye molecules could produce susceptibility effects responsible for the good detail apparent in gradient echo images. Further exploitation of this contrast mechanism to reveal microscopic structures is the topic of active research.

Histological stains typically do not possess native paramagnetic properties, and in this regard, luxol fast blue is unique. The solution longitudinal relaxation rates of LFB are a fraction of gadolinium analogues, but LFB's efficacy lies in its myelin specificity. The small magnetic moment of copper, due to its spin of 3/2 versus gadolinium's spin of 7/2, limits the relaxivity of LFB. This problem could be ameliorated by replacing the copper in LFB with a metal having a larger magnetic moment, such as manganese. A tetra sodium salt of manganese tetra-sulfo-phthalocyanine (MnPcS4) has been synthesized and measured to have a longitudinal relaxivity twice that of Gd-DTPA at 1.5 T (Saini et al., 1995). In a similar fashion, following a modified method of Webber and Busch (1965), LFB-chelated manganese could be synthesized to produce a more effective, white matter specific MR contrast agent.

While mapping myeloarchitectonics may be sufficient to delineate 50, 100, or more cortical subdivisions (Clark et al., 1992; Annese et al., 2004), complementary information, such as neuronal density, would provide a more holistic view of brain cytoarchitecture with MR microscopy. Clever synthetic chemistry schemes can be envisioned to create additional MR-visible, target-specific stains.

These new stains have applications in many areas of neuroscience. Target-specific stains, when paired with high resolution data, could lead to improved MR identification and segmentation of adjacent Brodmann areas, which differ in myelination and cell density (Brodmann, 1909). Regions of distinct cytoarchitecture could then be used to create more accurate, probabilistic-based MR atlases. With concomitant advances in magnetic field strength and radiofrequency coil technology, perhaps activation in functional imaging studies may then be localized to specific lamina instead of to broad regions.

In addition, these agents will facilitate the use of non-destructive, three-dimensional *ex vivo* imaging methods as a supplement—or alternative—to traditional histology methods used for pathological analysis of the brain. An arsenal of target-specific contrast agents could be used to investigate a variety of neurodegenerative diseases. LFB may be especially useful in investigating structural changes in demyelinating disorders, such as multiple sclerosis (MS), because of its chemical affinity for myelinated tissues. Contrast-enhanced *ex vivo* scans may help determine which imaging sequence and parameter selection best highlight pathologies *in vivo*. Furthermore, dual MR-optical contrast agents, such as LFB, will enable histological correlations to investigate what structural changes are visible with MR.

Acknowledgments

We thank Matthew Frosch and Jean Augustinack for assistance with samples, George Dai and Dika Kuljis for technical support, and Florian Eichler for critical reading of this manuscript. Support for this research was provided in part by the National Institutes of Health (NIH) Neuroimaging Training Grant Fellowship (T32EB001680) to Megan Blackwell, the National Center for Research Resources (NCRR)(P41-RR14075, and the NCRR BIRN Morphometric Project BIRN002, U24 RR021382), the National Institute for Biomedical Imaging and Bioengineering (R01 EB001550, R01EB006758), the National Institute for Neurological Disorders and Stroke (R01 NS052585-01), the Mental Illness and Neuroscience Discovery (MIND) Institute, and the National Alliance for Medical Image Computing (NAMIC, which is funded through the NIH Roadmap for Medical Research Grant U54 EB005149). Additional support was provided by The Autism & Dyslexia Project funded by the Ellison Medical Foundation.

References

Annese, J., Pitiot, A., Dinov, I.D., Toga, A.W., 2004. A myelo-architectonic method for the structural classification of cortical areas. Neuroimage 21 (1), 15–26.
Augustinack, J.C., van der Kouwe, A.J., Blackwell, M.L., Salat, D.H., Wiggins, C.J., Frosch, M.P., Wiggins, G.C., Potthast, A., Wald, L.L., Fischl, B.R., 2005. Detection of entorhinal layer II using 7Tesla magnetic resonance imaging. Ann. Neurol. 57, 489–494.
Barbier, E.L., Marrett, S., Danek, A., Vortmeyer, A., van Gelderen, P., Duyn, J., Bandettini, P., Grafman, J., Koretsky, A.P., 2002. Imaging cortical anatomy by high-resolution MR at 3.0 T: detection of the stripe of Gennari in visual area 17. Magn. Reson. Med. 48, 735–738.
Benveniste, H., Einstein, G., Kim, K.R., Hulette, C., Johnson, G.A., 1999. Detection of neuritic plaques in Alzheimer's disease by magnetic resonance microscopy. Proc. Natl. Acad. Sci. U. S. A. 96, 14079–14084.
Blamire, A.M., Rowe, J.G., Styles, P., McDonald, B., 1999. Optimising imaging parameters for post mortem MR imaging of the human brain. Acta Radiol. 40, 593–597.
Bloembergen, N., Purcell, E.M., Pound, R.V., 1948. Relaxation effects in nuclear magnetic resonance absorption. Phys. Rev. 73, 679–712.
Bloom, G., Kelly, J.W., 1960. The copper phthalocyanin dye “Astrablau” and its staining properties, especially the staining of mast cells. Histochemistry 2, 48–57.
Braak, H., 1976. On the striate area of the human isocortex. A golgi- and pigmentarchitectonic study. J. Comp. Neur. 166, 341–364.
Brodmann, K., 1909. Localization in the Cerebral Cortex, Trans. Garey, L.J., 1999. Imperial College Press, London.
Cacheris, W.P., Quay, S.C., Rocklage, S.M., 1990. The relationship between thermodynamics and the toxicity of gadolinium complexes. Mag. Reson. Imag. 8, 467–481.
Clare, S., Bridge, H., 2005. Methodological issue relating to in vivo cortical myelography using MRI. Hum. Brain Mapp. 26, 240–250.
Clark, V.P., Courchesne, E., Grafe, M., 1992. In vivo myeloarchitectonic analysis of human striate and extrastriate cortex using magnetic resonance imaging. Cereb. Cortex 2, 417–424.
Damasio, H., Kuljis, R.O., Yuh, W., van Hoesen, G.W., Ehrhardt, J., 1991. Magnetic resonance imaging of human intracortical structure *in vivo*. Cereb. Cortex 1, 374–379.
Eickhoff, S., Walters, N.B., Schleicher, A., Kril, J., Egan, G.F., Zilles, K., Watson, J.D.G., Amunts, K., 2005. High-resolution MRI reflects myeloarchitecture and cytoarchitecture of human cerebral cortex. Hum. Brain Mapp. 24, 206–215.
Fatterpekar, G.M., Naidich, T.P., Delman, B.N., Aguinaldo, J.G., Gultekin, S.H., Sherwood, C.C., Hof, P.R., Drayer, B.P., Fayad, Z.A., 2002. Cytoarchitecture of the human cerebral cortex: MR microscopy of excised specimens at 9.4 Tesla. Am. J. Neuroradiol. 23, 1313–1321.
Geisler, S., Heilmann, H., Veh, R.W., 2002. An optimized method for simultaneous demonstration of neurons and myelinated fiber tracts delineation of individual trunco- and palliothalamic nuclei in the mammalian brain. Histochem. Cell Biol. 117, 69–79.
George, R.D., Snow, A.W., Shirk, J.S., Barger, W.R., 1998. The alpha substitution effect on phthalocyanine aggregation. J. Porphy. Phthalocyanines 2, 1–7.
Hinds, O.P., Rajendran, N., Polimeni, J.R., Augustinack, J.C., Wiggins, G., Wald, L.L., Rosas, H.D., Potthast, A., Schwartz, E.L., Fischl, B., 2008. Accurate prediction of V1 location from cortical folds in a surface coordinate system. Neuroimage 39, 1585–1599.
Horobin, R.W., 2002. Phthalocyanines, porphyrins, and related aza[18]annulenes. In: Horobin, R.W., Kiernan, J.A. (Eds.), Conn's Biological Stains: A Handbook of Dyes, Stains, and Fluorochromes for Use in Biology and Medicine. BIOS Scientific Publishers, Oxford, pp. 379–388.
Innocenti, G.M., Manger, P.R., Masiello, I., Colin, I., Tettoni, L., 2002. Architecture and callosal connections of visual areas 17, 18, 19 and 21 in the ferret (mustela putorius). Cereb. Cortex 12, 411–422.
Jarvis, K.E., 1992. Handbook of Inductively Coupled Plasma Mass Spectrometry. Chapman and Hall, New York.
Johnson, G.A., Cofer, G.P., Gewalt, S.L., Hedlund, L.W., 2002. Morphologic phenotyping with magnetic resonance microscopy: the visible mouse. Radiology 222, 789–793.
Kety, S.S., 1951. The theory and applications of the exchange of inert gas at the lungs and tissues. Pharmacol. Rev. 3, 1–41.
Kiernan, J.A., 1999. Histological & Histochemical Methods: Theory and Practice, 3rd ed. Butterworth Heinemann, Oxford.
Klüver, H., 1944. On naturally occurring porphyrins in the central nervous system. Science 99, 482–484.
Klüver, H., Barrera, E., 1953. A method for the combined staining of cells and fibers in the nervous system. J. Neuropathol. Exp. Neurol. 12, 400–403.
Koenig, H., 1959. The proteolipid nature of the neurokeratin network of myelin. J. Neurochem. 4, 93–100.
Lauffer, R.B., 1987. Paramagnetic metal complexes as water proton relaxation agents for NMR imaging: theory and design. Chem. Rev. 87, 901–927.
Lord Rayleigh, 1874. On the manufacture and theory of diffraction gratings. Philos Mag 47, 81–93, 193–205.
Manoonkitiwongsa, P.S., Jackson-Friedman, C., McMillan, P.J., Schultz, R.L., Lyden, P.D., 2001. Angiogenesis after stroke is correlated with increased numbers of macrophages: the clean-up hypothesis. J. Cereb. Blood Flow Metab. 21, 1223–1231.

Nauta, W.J.H., Freitag, M., 1986. Fundamental neuroanatomy. Freeman, New York.
Oros-Peusquens, A.M., Shah, N.J., Amunts, K., Zilles, K., 2003. Optimised high resolution MRI of the post mortem brain, 2003. NeuroImage 19, e1458–e1460 (Suppl).
Pearse, A.G.E., 1955. Copper phthalocyanins as phospholipids stains. J. Pathol. Bacteriol. 70, 554–557.
Pfefferbaum, A., Sullivan, E.V., Adalsteinsson, E., Garrick, T., Harper, C., 2004. Postmortem MR imaging of formalin-fixed human brain. NeuroImage 21, 1585–1595.
Pisani, L.J., Ross, A.B., Diedrich, C.J., Nau, W.H., Glover, G.H., Sommer, F.G., Butts, K., 2004. Optimizing spatial resolution for mr thermal imaging of transurethral ultrasound prostrate ablation. 14th Scientific Meeting of the International Society for Magnetic Resonance in Medicine, Kyoto, Japan.
Press, W.H., Flannery, B.P., Teukolsky, S.A., Vetterling, W.T., 1988. Numerical Methods in C. Cambridge University Press, Cambridge.
Press, G.A., Amaral, D.G., Squire, L.R., 1989. Hippocampal abnormalities in amnesic patients revealed by high-resolution magnetic resonance imaging. Nature 341, 54–57.
Saeed, M., Higgins, C.B., Geschwind, J.F., Wendland, M.F., 2000. T1-relaxation kinetics of extracellular, intracellular and intravascular MR contrast agents in normal and acutely reperfused infarcted myocardium using echo-planar MR imaging. Eur. Radiol. 10, 310–318.
Saini, S.K., Jena, A., Dey, J., Sharma, A.K., Singh, R., 1995. MnPcS4: a new MRI contrast enhancing agent for tumor localization in mice. Magn. Reson. Imag. 13, 985–990.
Salthouse, T.N., 1962. Reversal of solubility characteristics of 'luxol' dye-phospholipid complexes. Nature 199: 821, 1963.
Scholtz, C.L., 1977. Quantitative histochemistry of myelin using luxol fast blue MBS. Histochem. J. 9, 759–765.
Shattuck, D., Sandor-Leahy, S., Schaper, K., Rottenberg, D., Leahy, R., 2001. Magnetic resonance image tissue classification using a partial volume model. NeuroImage 13, 856–876.
Tovi, M., Ericsson, A., 1992. Measurements of T1 and T2 over time in formalin-fixed human whole-brain specimens. Acta Radiol. 33, 400–404.
Ungerleider, Desimone, 1986. Projections to the superior temporal sulcus from the central and peripheral field representations of V1 and V2. J. Comp. Neurol. 248, 147–163.
Vogt, C., Vogt, O., 1942. Morphologische Gestaltungen unter normalen und pathogenen Bedingungen. J. Psychol. Neurot. 50, 161–524.
von Economo, C., Koskinas, G.N., 1925. Die Cytoarchitektonik der Hirnrinde des Erwaschsenen Menschen. Springer, Vienna.
Walters, N.B., Egan, G.F., Kril, J.J., Kean, M., Waley, P., Jenkinson, M., Watson, J.D.G., 2003. In vivo identification of human cortical areas using high-resolution MRI: an approach to cerebral structure–function correlation. Proc. Natl. Acad. Sci. U. S. A. 100, 2981–2986.
Webber, J.H., Busch, D.H., 1965. Complexes derived from strong field ligands. XX. The effect of extraplanar ligands on the properties of transition metal 4,4′,4″,4‴-tetrasulfophthalocyanines. Inorg. Chem. 4, 469–471.